

Integrated bi-directional focusing and tracking actuators in a monolithic device for a MEMS optical pick-up head

This article has been downloaded from IOPscience. Please scroll down to see the full text article.

2006 J. Micromech. Microeng. 16 1290

(<http://iopscience.iop.org/0960-1317/16/7/024>)

View [the table of contents for this issue](#), or go to the [journal homepage](#) for more

Download details:

IP Address: 140.114.59.160

The article was downloaded on 21/08/2012 at 05:31

Please note that [terms and conditions apply](#).

Integrated bi-directional focusing and tracking actuators in a monolithic device for a MEMS optical pick-up head

Mingching Wu and Weileun Fang

Department of Power Mechanical Engineering, National Tsing Hua University, Hsinchu, Taiwan

E-mail: fang@pme.nthu.edu.tw

Received 13 February 2006, in final form 5 April 2006

Published 17 May 2006

Online at stacks.iop.org/JMM/16/1290

Abstract

This work presents a miniaturized two-degree-of-freedom (2-DOF) optical pick-up head implemented using MEMS technology. This device contains novel bi-directional vertical comb-drive actuators to act as the focusing positioner, and V-beam thermal actuators to serve as the tracking positioner. In addition, a UV-cured polymer droplet is used for an objective lens. Particularly, the focusing and tracking actuators are monolithically fabricated and integrated in a single device. Electrical routing and isolation is also available by poly-Si and Si₃N₄ multi-layers for 2-DOF operation. In applications, the proposed device has been successfully fabricated and characterized. The upward and downward displacements of the focusing optical pick-up head are 4.6 μm and 4.1 μm , respectively, at a 30 V driving voltage. And the in-plane displacement of the tracking optical pick-up head is $\pm 16.3 \mu\text{m}$, at a 5 V driving voltage. The resonant frequencies of the focusing and tracking systems are 1.9 kHz and 4.1 kHz, respectively.

(Some figures in this article are in colour only in the electronic version)

1. Introduction

Due to the rapid growth of information technology, small and high capacities are the requirements of state-of-the-art data storage system. Recently, several approaches to obtain high-density data storage have been widely investigated on the basis of MEMS technologies such as magnetic hard disk drives [1–3], magnetic-optical recording [4] and AFM tip recording [5, 6]. To increase the data storage density of the optical data storage system is also another design consideration. Particularly, employing the plastic optical disk for removable recording media is more cost-effective than the other technologies. The high numerical aperture (NA) optical system substantially increases the storage density in terms of the smaller optical spot. However, such high storage density requires a very high bandwidth servo-tracking system to precisely position the optical pick-up head within a narrow track spacing ($\sim 100 \text{ nm}$). One promising solution is to employ the MEMS actuator with higher response bandwidth for nano-scale positioning [1].

The development of an optical pick-up head using MEMS technology has been extensively demonstrated. In general, the optical pick-up head mainly consists of focusing components (focusing actuator, spring, etc), tracking components (tracking actuator, springs, etc) and optical components (lens, lens holder, etc). Various optical elements have been miniaturized and integrated by means of micromachining processes, such as high NA diffractive optical elements [7], polymer-based optical elements [8] and micro optical bench [9]. The focusing and tracking components are flexible only in the out-of-plane direction and the in-plane direction, respectively. It is difficult to monolithically fabricate and integrate the focusing and tracking components on a single chip. The piezoelectric actuators [10] and bimorph thermal actuators [11] have been exploited for data tracking. Moreover, electrostatic vertical comb-drive actuators for optical focusing have been demonstrated in [12, 13]. In addition, the concept of integrating UV-cured polymer lenses with MEMS actuators has also been demonstrated in [14], and the in-plane and out-of-plane

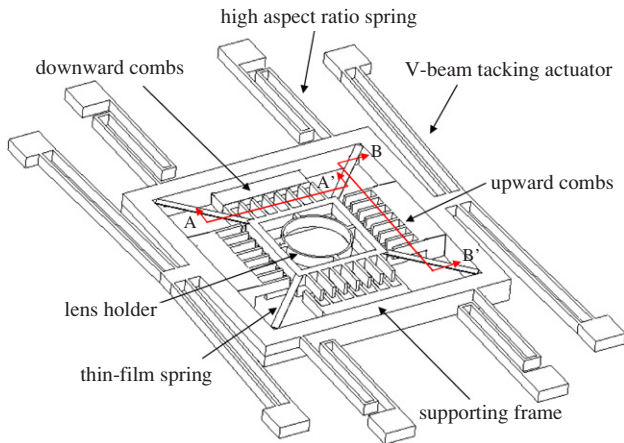


Figure 1. Schematic of the proposed 2-DOF optical pick-up head.

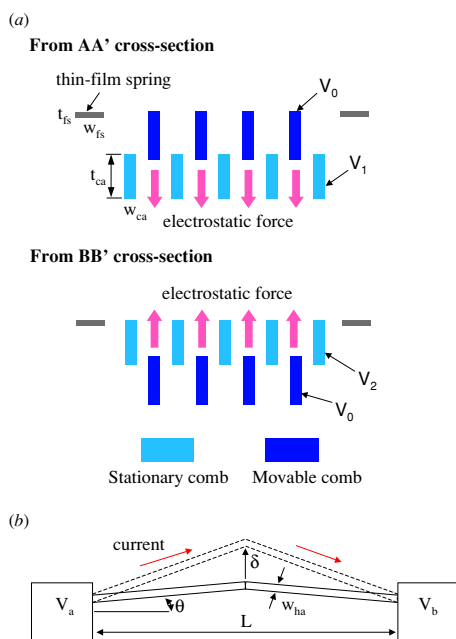


Figure 2. (a) Concept of the bi-directional vertical comb-drive actuator and (b) the parameter definitions of the V-beam thermal actuator.

positioning actuators are integrated by means of a bonding technique.

This work attempts to develop a novel two degree-of-freedom (2-DOF) optical pick-up head, where the key components are monolithically fabricated and integrated in a single device by means of process integration. This device contains novel bi-directional vertical comb-drive actuators to act as the focusing positioner, and V-beam thermal actuators to serve as the tracking positioner. In addition, the UV-cured polymer droplet is used for the objective lens. In short, the present design has the potential to match the requirements of small-form-factor (SFF) optical data storage systems.

2. Concepts and design

The concept of the presented 2-DOF micromachined optical pick-up head is shown in figure 1. This MEMS device

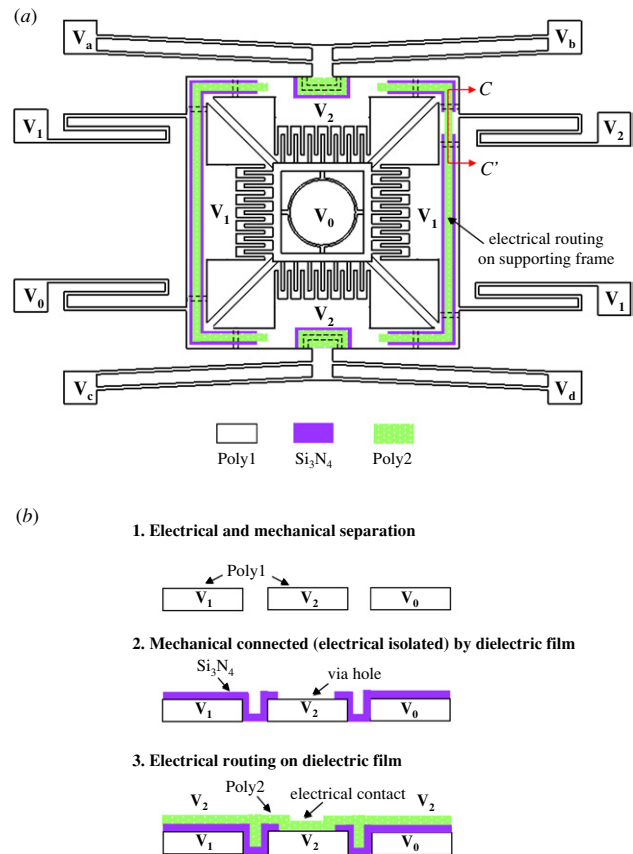


Figure 3. The concept of electrical routing and isolation. (a) Top view of various electrical potentials provided by separate Poly1 structures, mechanically connected but electrically isolated by the Si_3N_4 film, and electrical routing by poly-Si and (b) cross section of CC' .

monolithically integrates bi-directional focusing (out-of-plane) actuators, V-beam tracking (in-plane) actuators, in-plane and out-of-plane springs, supporting frame and lens holder. The UV-cured polymer lens can be integrated on the lens holder after releasing the device, so that the incident light beam can be focused by the UV polymer lens and modulated by focusing and tracking actuators. The lens holder is connected to the stationary rigid supporting frame by four thin-film springs. The vertical comb electrodes are placed at the supporting frame and the lens holder to form bi-directional focusing actuators (named upward and downward combs in figure 1). Thus, the out-of-plane position of the lens, no matter in the upward or downward direction, can be tuned. In addition, the lens holder and supporting frame are connected to an Si substrate by V-beam thermal actuators and four high aspect ratio springs. Therefore, the in-plane position of a lens can be tuned by V-beam thermal actuators. The monolithically integrated focusing and tracking actuators can be independently operated by the design of electrical routing and isolation.

2.1. Bi-directional focusing actuators

As indicated in figure 1, the moving electrodes of the upward comb are located below the stationary electrodes, whereas the moving electrodes of the downward comb are located above the

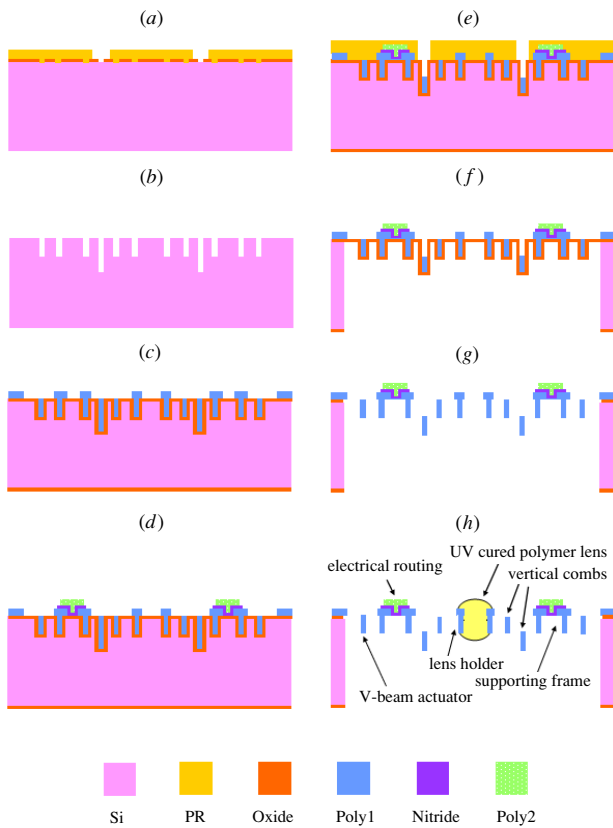


Figure 4. Fabrication process steps. (a) Self-aligned etching mask, (b) DRIE for two different depths, (c) fully refill trenches, (d) electric routing and isolation, (e) 3rd DRIE trimming, (f) backside DRIE, (g) removing passivation and (h) the dropped polymer lens.

stationary electrodes. The monolithically integrated stationary electrodes of the upward and downward combs are electrically isolated and can be actuated individually, and the moving electrodes are grounded through thin-film springs. Figure 2(a) shows the cross sections of AA' and BB' in figure 1. The downward motion is actuated by V_0 and V_1 , while the upward motion is actuated by V_0 and V_2 . Moreover, the thickness and location of the vertical comb electrodes are tunable by the process to improve the traveling distance and the driving voltage [15]. In this design, the thicknesses t_{ca} of both movable combs and stationary combs are $20\ \mu\text{m}$.

The traveling distance of the focusing actuator would be limited by the side-sticking effect due to the misalignment of the comb electrodes [16]. In this work, the self-aligned vertical combs technique is adopted to prevent the misalignment of the electrodes [17]. In addition, the in-plane to out-of-plane stiffness ratio of the thin-film spring in figure 1 will also influence the occurrence of side sticking. The in-plane to out-of-plane stiffness ratio K_{ratio} of thin-film spring with thickness t_{fs} and width w_{fs} is $(w_{fs}/t_{fs})^2$. In this design, the dimensions of w_{fs} and t_{fs} are $20\ \mu\text{m}$ and $2\ \mu\text{m}$, respectively, so that K_{ratio} is nearly 100. Therefore, the thin-film spring is flexible enough for vertical actuation and stiff enough to suppress the side-sticking effect.

In optical consideration, a larger objective lens has various advantages. For instance, a larger objective lens can increase the working distance and the misalignment problem becomes

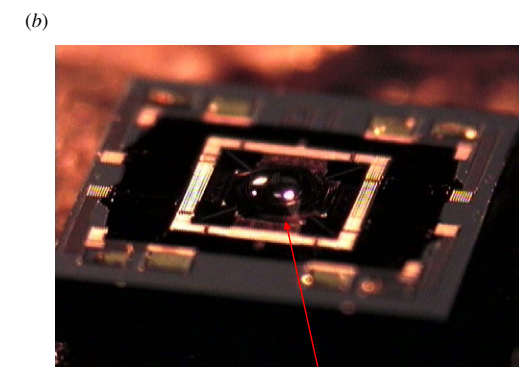
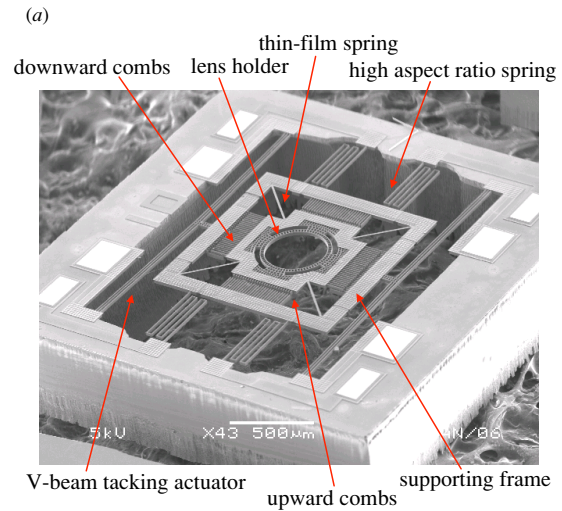


Figure 5. Fabrication result of the 2-DOF optical pick-up head: (a) without and (b) with a UV-cured polymer lens.

less critical as well. Meanwhile, the mass of the lens is increased, so as to influence the design of focusing actuators. In the present work, the UV-cured polymer lens suspended by thin-film springs has an initial out-of-plane deflection δ due to gravity. Thus, the location of the vertical comb electrodes is influenced by the vertical deflection δ , so that the traveling distance and driving voltage are also changed. For the case of BB' cross section of figure 2(a), the driving voltage will be significantly increased if the deflection d is greater than the initial engagement of stationary and movable combs. This gives design constraints to the lens size, spring stiffness and comb thickness.

2.2. V-beam tracking actuators

As figure 1 shows, the present device employs the V-beam thermal actuators [18] for in-plane tracking. After the thermal expansion of the V-beam by joule heating, the actuator will push the supporting frame and the focusing system in the in-plane direction. The traveling distance δ of actuator is determined by the length L and the angle θ of the V-beam, as indicated in figure 2(b) [18]. The V-beam actuators located on both sides of the lens holder could move the light beam in the opposite direction. Moreover, the V-beams together with four high aspect ratio springs also serve as the suspension of the whole device. In this design, the spring width w_{hs} is $2\ \mu\text{m}$

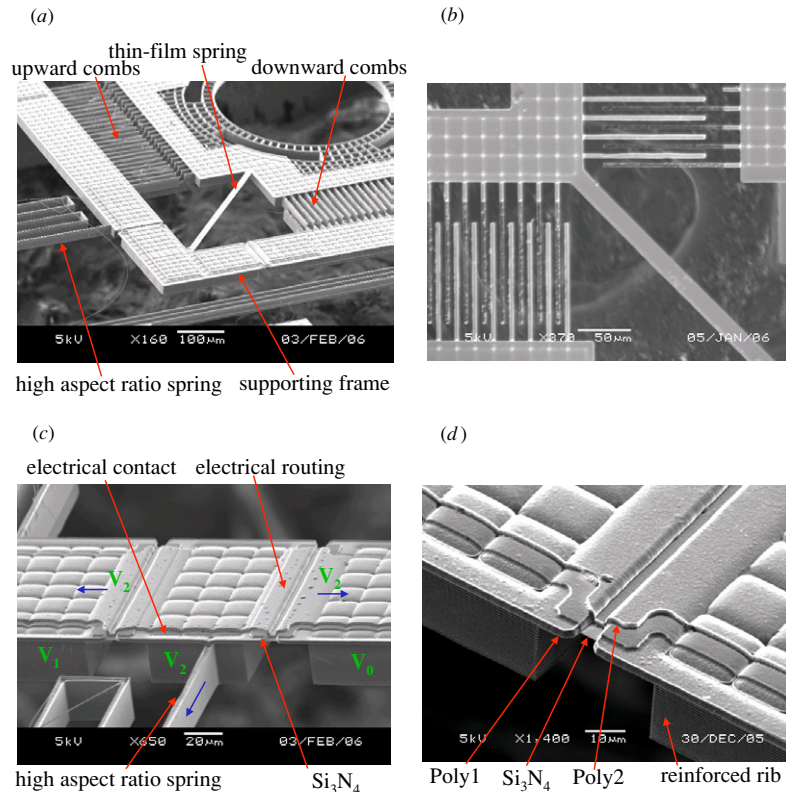


Figure 6. (a) A bird's eye view of the proposed device, (b) top view of the self-aligned comb electrodes, (c) the electrical routing and isolation and (d) the poly-Si and Si₃N₄ multi-layers.

and thickness t_{hs} is 20 μm , so that the in-plane to out-of-plane stiffness ratio K_{ratio} is nearly 0.01. Therefore, the high aspect ratio spring is flexible enough for in-plane actuation, and stiff enough to suspend the device.

2.3. Electrical routing and isolation

The stacking of two conducting poly-Si layers (named Poly1 and Poly2) and one insulation Si₃N₄ film is employed in this study to form various electrical potential regions during operation, as shown in figure 3. Thus, the focusing and tracking components of the present device are operated independently. The device in figure 3(a) is monolithically fabricated using the Poly1 layer. The dash lines indicate the areas where the Poly1 is removed, and the whole device is divided into several separate regions. After depositing with Si₃N₄ films, these separated regions are mechanically connected but electrically isolated, as depicted by the CC' cross section in figure 3(b). The Poly2 film is further employed to act as an electrical routing. For instance, the Poly2 electrical routings defined using microfabrication can pass through the supporting frame and the high aspect ratio springs to connect the focusing actuators to bonding pads, as shown in figure 3(a). In summary, the device has three electrical potential regions (V_0 – V_2) for bi-directional focusing actuation, and also has four electrical potential regions (V_a – V_d) for tracking actuation.

3. Fabrication and results

The fabrication processes employed in this study are illustrated in figure 4. The processes began with the growth and

patterning of thermal oxide, as shown in figure 4(a). A second photolithography was used to define the location of deeper trenches. The patterned thermal oxide and photoresist were used as the self-aligned etching masks for the following DRIE (deep reactive ion etching). The photoresist in figure 4(a) was removed after the first DRIE. The silicon oxide acted as the etching mask for the second DRIE. The silicon substrate had self-aligned trenches with two different thicknesses (shallow and deep trenches) for vertical comb electrodes after the second DRIE, as shown in figure 4(b) [17]. After that, these trenches were fully refilled by thermal oxide and the first LPCVD (low pressure chemical vapor deposition) poly-Si (i.e. Poly1) films. The main structures were all available by the Poly1 layer and etched into various separate regions for individual electrical potentials, as shown in figure 4(c). After the Poly1 was patterned, the Si₃N₄ insulation layer and the second poly-Si film (i.e. Poly2) were deposited and patterned to achieve the electrical routing and isolation in a monolithic device, as shown in figure 4(d). The Poly2 layer could act as the electrical interconnection for electrically isolated comb electrodes. After patterned with photoresist, the third DRIE was exploited to trim the thickness of refilled Poly1 in deep trench, as shown in figure 4(e). The initial engagement of comb electrodes was then defined. Hence the micromachined structures located at different out-of-plane positions became available, so as to realize the vertical comb electrodes. In addition, the V-beam thermal actuators and the lens holder were also implemented using the refilled Poly1 in shallow trenches. The backside thermal oxide was patterned as the etching mask, and the Si substrate was then fully removed

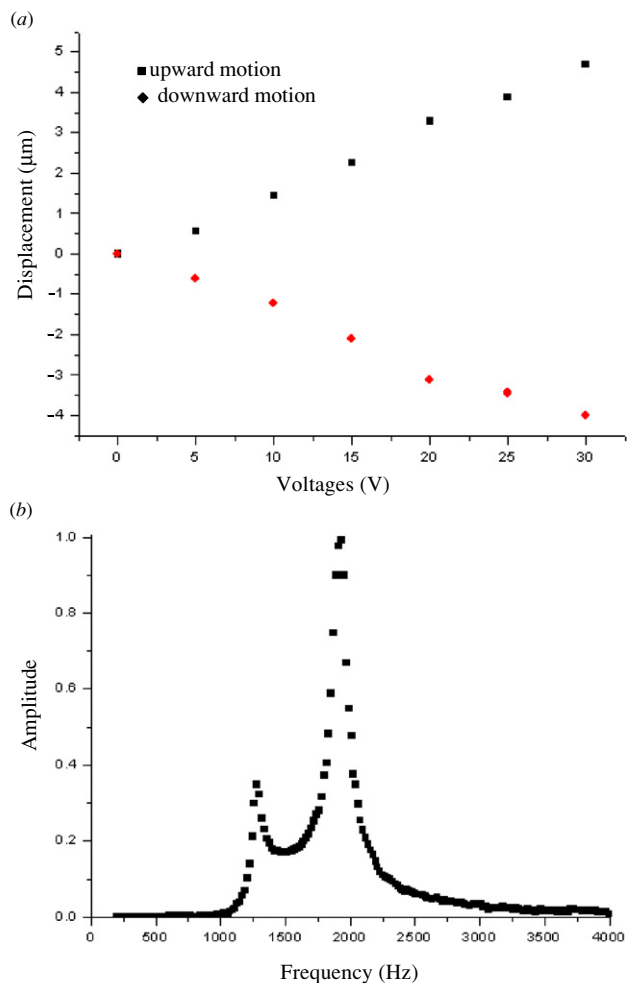


Figure 7. Measured results from the focusing components of the device shown in figure 5(a): (a) the static load-deflection test for upward and downward actuations and (b) the frequency response of the device.

from the backside by DRIE, as shown in figure 4(f). The front-side thermal oxide performed as passivation and etch-stop layers for the poly-Si structure during the DRIE silicon etching. A through hole was also available for the incident light to pass through the wafer. Finally, the passivation layers were removed and the UV-cured polymer droplet was dropped to the lens holder, as shown in figures 4(g) and (h).

The 2-DOF optical pick-up head is successfully demonstrated in figure 5. The SEM photo in figure 5(a) clearly shows the components of the lens holder, supporting frame, V-beam thermal actuators, vertical comb actuators and springs. Figure 5(b) indicates that the device after the UV-cured polymer droplet was dropped to the lens holder to act as the objective lens. The zoom in the photo in figure 6(a) shows the upward and downward comb actuators. The initial engagement of comb electrodes available by the third DRIE trimming is $3 \mu\text{m}$ to provide a larger electro-statically driving force. The thickness of the thin-film spring defined by Poly1 was $t_{fs} = 2 \mu\text{m}$, and the thickness of the high aspect ratio spring defined by refilled Poly1 in shallow trenches was $t_{hs} = 20 \mu\text{m}$. The $20 \mu\text{m}$ thick refilled Poly1 also formed the reinforced ribs at the backside of supporting frame

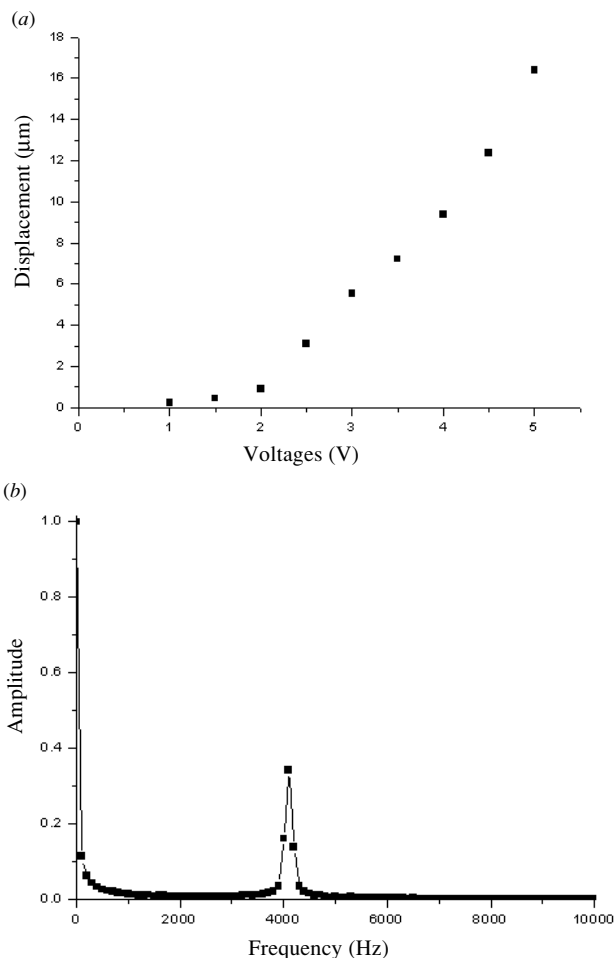


Figure 8. Measured results from the tracking components of the device shown in figure 5(a): (a) the static load-deflection test for in-plane actuation and (b) the frequency response of the device.

and the lens holder to substantially improve their stiffness. Figure 6(b) shows the perfect alignment of the stationary and moving comb electrodes using the present processes. Therefore, the side-sticking effect can be suppressed. Figures 6(c) and (d) indicate the fabrication result of electrical routing illustrated in figure 3(b). It is clearly observed that the separate Poly1 structures are mechanically connected by the Si_3N_4 layer. It is also observed that the Poly2 film is on the top of the Si_3N_4 insulation layer for electrical routing. Moreover, the high aspect ratio spring and reinforced ribs are clearly demonstrated in the zoom in the photos of figures 6(c) and (d).

4. Testing

To demonstrate the performance of the presented 2-DOF optical pick-up head, the static and dynamic characteristics of the fabricated MEMS devices were characterized. The device was driven by dc voltage for static load-deflection test, and driven by ac voltage for dynamic resonant test. The out-of-plane static displacement of the focusing components was measured by the optical interferometer. An optical

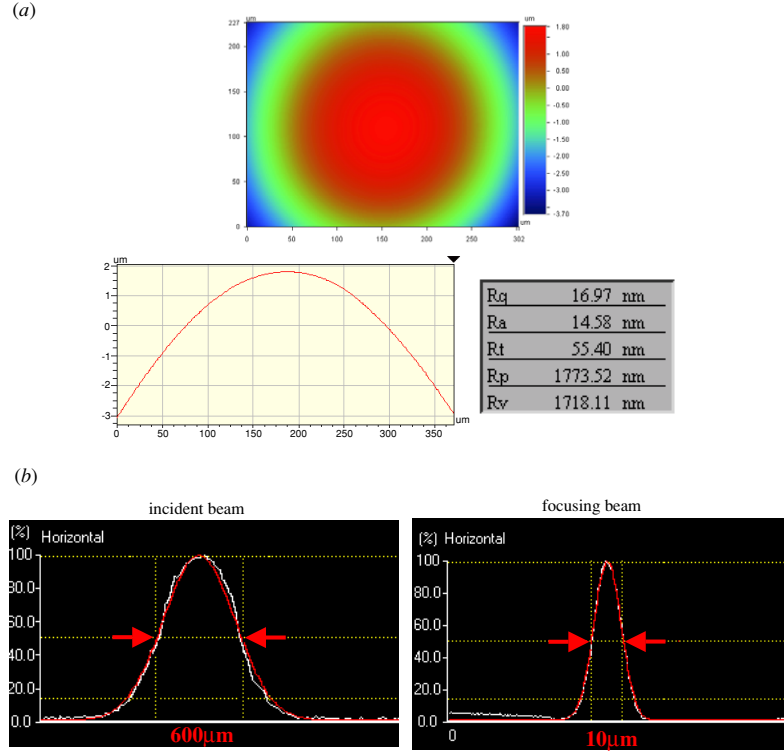
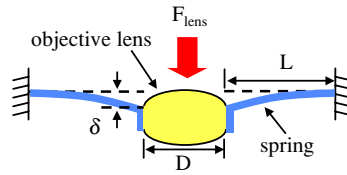


Figure 9. Optical property of a UV-cured polymer droplet lens: (a) the surface roughness of the lens measured by an optical interferometer and (b) the intensity profiles of the incident beam and the focusing beam.

Table 1. Initial out-of-plane deflection induced by the weight of the UV-cured polymer lens.



	Lens weight	Lens A diameter: 200 μm mass: $\sim 10 \mu\text{g}$	Lens B diameter: 400 μm mass: $\sim 50 \mu\text{g}$	Lens C diameter: 600 μm mass: $\sim 200 \mu\text{g}$
Spring length				
Spring A: L = 200 μm ,		$\delta = 0.03 \mu\text{m}$	$\delta = 0.16 \mu\text{m}$	$\delta = 0.64 \mu\text{m}$
Spring B: L = 300 μm		$\delta = 0.11 \mu\text{m}$	$\delta = 0.53 \mu\text{m}$	$\delta = 2.12 \mu\text{m}$
Spring C: L = 400 μm		$\delta = 0.25 \mu\text{m}$	$\delta = 1.25 \mu\text{m}$	$\delta = 5 \mu\text{m}$

Note: $w_s = 20 \mu\text{m}$, $t_s = 2 \mu\text{m}$

laser Doppler vibrometer was used to measure the out-of-plane dynamic response of the focusing system. Figure 7 shows the typical measured results from the device shown in figure 5(a). As shown in figure 7(a), the maximum upward and downward displacements of the device were $4.6 \mu\text{m}$ and $4.1 \mu\text{m}$, respectively, when the driving voltage reached 30 V. Figure 7(b) shows the frequency response of the device. The resonant frequency associated with the first out-of-plane spring bending mode is 1.9 kHz.

Table 1 shows the initial out-of-plane deflection δ after the UV-cured polymer droplet was dropped to the lens holder. There are three different lenses ($D = 200\text{--}600 \mu\text{m}$) and spring lengths ($L = 200\text{--}400 \mu\text{m}$) during the measurement. The

measured lens weight ranges from $10 \mu\text{g}$ to $200 \mu\text{g}$ when the lens holder increases from $200 \mu\text{m}$ to $600 \mu\text{m}$. The largest vertical deflection δ can even reach $5 \mu\text{m}$ for $R = 600 \mu\text{m}$ lenses and $L = 400 \mu\text{m}$ springs. In this case, the stroke of the downward vertical comb actuators is significantly reduced, whereas the driving voltage of the upward vertical comb actuators is significantly increased. This is a typical example to show the design considerations for the lens size, spring stiffness and comb thickness.

Moreover, the in-plane displacement of the tracking system was measured using an image captured approach by a commercial micro motion analyzer. Figure 8 also shows the typical measured results of the device shown in

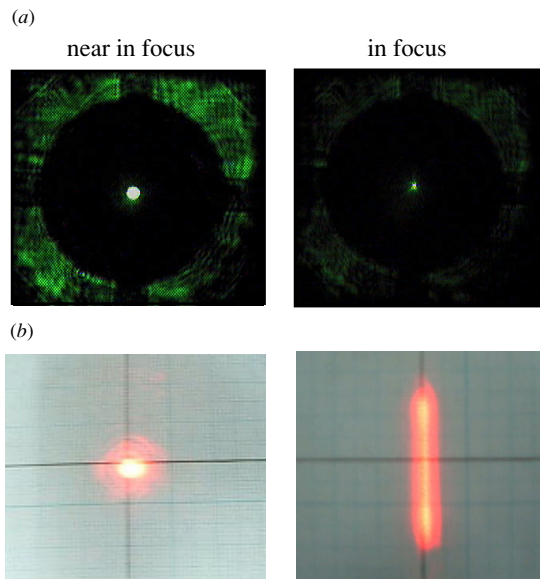


Figure 10. Optical test using the device shown in figure 5(b): (a) variation of the laser spot during the focusing test and (b) the scanning line generated during the tracking test.

figure 5(a). As shown in figure 8(a), the in-plane displacement of the device driven by the single-side V-beam actuator was $16.3 \mu\text{m}$ when the applied voltage was 5 V. The frequency response in figure 8(b) shows that the first in-plane mode of a typical tracking device is 4.1 kHz. It indicates that the MEMS device has a faster response as well as a higher bandwidth for the servo-tracking system, as compared with a conventional optical pickup head.

The optical properties of a UV-cured polymer droplet lens are indicated in figure 9. Figure 9(a) shows the surface profile of a polymer lens measured using an optical interferometer. The surface roughness of the polymer lens is 14.6 nm. Therefore, the polymer lens provided a good surface for optical applications. In addition, the intensity profile of a focused beam measured using the beam profiler is indicated in figure 9(b). During the test, a laser beam was incident on the UV-cured polymer lens from the backside of the substrate, and then focused on a beam profiler by the polymer lens. The spot sizes for the incident beam and the focusing beam were $\sim 600 \mu\text{m}$ and $\sim 10 \mu\text{m}$ (full width at half maximum), respectively. Since the focused spot size of the available polymer lens still cannot satisfy the optical requirements, a high NA commercial lens is required. Thus, the optical properties of the miniaturized MEMS pickup can be significantly improved. In this regard, the lens will integrate to the lens holder by means of assembly.

To demonstrate the optical modulation of the presented device, a laser beam was incident on the polymer droplet lens of the device in figure 5(b) from the backside of the substrate and then focused on a microscope objective lens. The photos in figure 10(a) show the variation of beam spot during focusing. The photos in figure 10(b) show the variation of beam spot during tracking, and the driving frequency was 15 Hz. The scanning range could be modulated by the dc voltages of V-beam tracking actuators.

5. Conclusions

This study has demonstrated a novel 2-DOF optical pick-up head. The focusing and tracking actuators are integrated in a monolithic micromachined device by means of process integration. The novel bi-directional vertical comb actuators act as the focusing positioner, and the V-beam thermal actuators serve as a tracking positioner. The upward and downward combs are initially engaged and self-aligned by the present process. The critical design of electrical routing and insulation is available by poly-Si and Si_3N_4 multi-layers. Moreover, the potential of electrically independent regions could be routing through the suspended springs to provide 2-DOF operations. The UV-cured polymer droplet lens is also integrated on the lens holder. In results, the upward and downward displacements of the focusing system are $4.6 \mu\text{m}$ and $4.1 \mu\text{m}$, respectively, at a dc driving voltage of 30 V. The in-plane displacement of the tracking system is $\pm 16.3 \mu\text{m}$, when a 5 V dc voltage is applied. The resonant frequency of focusing and tracking systems are 1.9 kHz and 4.1 kHz, respectively. In applications, the present 2-DOF optical pick-up head with faster response and smaller size can match the requirements of small-form-factor optical data storage.

Acknowledgments

This paper was (partially) supported by the Ministry of Economic Affairs, Taiwan, under contract 94-EC-17-A-07-S1-0011, and by Nation Science Council, Taiwan, under contract NSC 94-2212-E-007-026. The authors would also like to thank the Center for Nano-Science and Technology in the Tsing Hua University (Taiwan), the Nano Facility Center of National Chiao Tung University (Taiwan) and the NSC National Nano Device Laboratory (Taiwan) for providing the fabrication facilities.

References

- [1] Fan L-S, Ottesen H H, Reiley T C and Wood R W 1995 Magnetic recording-head positioning at very high track densities using a microactuator-based, two-stage servo system *IEEE Trans. Ind. Electron.* **42** 222–33
- [2] Hirano T, Fan L-S, Gao J Q and Lee W Y 1998 MEMS milliactuator for hard-disk-drive tracking servo *J. Microelectromech. Syst.* **7** 149–55
- [3] Toshiyoshi H, Mita M and Fujita H 2002 A MEMS piggyback actuator for hard-disk drives *J. Microelectromech. Syst.* **11** 648–64
- [4] Hata S, Yamada Y, Ichihara J and Shimokohbe A 2002 A micro lens actuator for optical flying head *IEEE MEMS'02 (Las Vegas, CA)* pp 507–10
- [5] Vettiger P *et al* 2002 The millipede—nanotechnology entering data storage *IEEE Trans. Nanotechnol.* **1** 39–55
- [6] Despont M, Drechsler U, Yu R, Pogge H B and Vettiger P 2004 Wafer-scale microdevice transfer/interconnect: its application in an AFM-based data-storage system *J. Microelectromech. Syst.* **13** 895–901
- [7] Lim J, Jeong G-B, Kim S-M, Han J, Yoo J-M, Park N-C and Kang S 2006 Design and fabrication of a diffractive optical element for the objective lens of a small form factor optical data storage device *J. Microelectromech. Syst.* **16** 77–82
- [8] Tseng F G and Hu H T 2003 A novel micro optical system employing inclined polymer mirrors and Fresnel lens for monolithic integration of optical disk pickup heads *IEEE Transducers'03 (Boston, MA)* pp 599–602

- [9] Lin L Y, Shen J L, Lee S S and Wu M C 1996 Realization of novel monolithic free-space optical disk pickup heads by surface-micromachining *Opt. Lett.* **21** 155–7
- [10] Yee Y, Nam H-J, Lee S-H, Bu J U, Jeon Y-S and Cho S-M 2000 PZT actuated micromirror for nano-tracking of laser beam for high-density optical data storage *IEEE MEMS'00 (Miyazaki, Japan)* pp 435–8
- [11] Yang J P, Deng X C and Chong T C 2005 An electro-thermal bimorph-based microactuator for precise track-positioning of optical disk drives *J. Micromech. Microeng.* **15** 958–65
- [12] Kim S-H, Yee Y, Choi J, Kwon H, Ha M-H, Oh C and Bu J U 2003 Integrated micro optical flying head with lens positioning actuator for small form factor data storage *IEEE Transducers'03 (Boston, MA)* pp 607–10
- [13] Kim S-H, Yee Y, Choi J, Kwon H, Ha M-H, Oh C and Bu J U 2004 A micro optical flying head for PCMCIA-sized optical data storage *IEEE MEMS'04 (Maastricht, The Netherlands)* pp 85–8
- [14] Kwon S, Milanović V and Lee L P 2002 Large-displacement vertical microlens scanner with low driving voltage *IEEE Photon. Technol. Lett.* **14** 1572–4
- [15] Tsai J M-L, Chu H-Y, Hsieh J and Fang W 2004 The BELST II process for silicon HARM vertical comb actuator and its applications *J. Micromech. Microeng.* **15** 535–42
- [16] Tsuboi O, Mizuno Y, Koma N, Soneda H, Okuda H, Ueda S, Sawaki I and Yamagishi F 2002 A rotational comb-driven micromirror with a large deflection angle and low drive voltage *IEEE MEMS'02 (Las Vegas, NV)* pp 532–5
- [17] Wu M and Fang W 2005 Design and fabrication of MEMS devices using the integration of MUMPs, trench-refilled molding, DRIE and bulk silicon etching processes *J. Micromech. Microeng.* **15** 535–42
- [18] Sinclair M J 2000 A high force low area MEMS thermal actuator *Inter Society Conf. on Thermal Phenomena (Las Vegas, NV)* pp 127–32